Influence of biologically inspired nanometer surface roughness on antigen–antibody interactions for immunoassay–biosensor applications

Paul V Tuttle IV[1]
Ann E Rundell[1]
Thomas J Webster[1,2,3]

[1]Weldon School of Biomedical
Engineering, and [2]School of Materials
Engineering, Purdue University,
West Lafayette, IN 47907, USA;
[3]Present address: Division of
Engineering, Brown University,
Providence, RI, USA

Abstract: Current research efforts to improve immunoassay–biosensor functionality have centered on detection through the optimal design of microfluidic chambers, electrical circuitry, optical sensing elements, and so on. To date, little attention has been paid to the immunoassay–biosensor membrane surface on which interactions between antibodies and antigens must occur. For this reason, the objective of the present study was to manipulate the nanometer surface roughness of a model immunoassay–biosensor membrane to determine its role on sensitivity and specificity. It was hypothesized that surface roughness characteristics similar to those used by the body's own immune system with B-lymphocyte cell membranes would promote antigen-antibody interactions and minimize non-specific binding. To test this hypothesis, polystyrene 96-well plate surfaces were modified to possess similar topographies as those of B-lymphocyte cell membranes. This was accomplished by immobilizing Protein A conjugated gold particles and Protein A conjugated polystyrene particles ranging in sizes from 40 to 860 nm to the bottom of polystyrene wells. Atomic force microscopy results provided evidence of well-dispersed immunoassay–biosensor surfaces for all particles tested with high degrees of biologically inspired nanometer roughness. Testing the functionality of these immunosurfaces using antigenic fluorescent microspheres showed that specific antigen capture increased with greater nanometer surface roughness while nonspecific antigen capture did not correlate with surface roughness. In this manner, results from this study suggest that large degrees of biologically inspired nanometer surface roughness not only increases the amount of immobilized antibodies onto the immunosurface membrane, but it also enhances the functionality of those antibodies for optimal antigen capture, criteria critical for improving immunoassay–biosensor sensitivity and specificity.

Keywords: nanometer surface roughness, antibody-antigen interaction, B-lymphocyte, immunosurface, immunoassay, biosensor

Introduction

There are numerous immunoassay–biosensor applications necessitating highly sensitive pathogen detection. For example, aerosolized *Bacillus anthracis* spores are odorless, invisible to the naked eye, have the potential to travel many kilometers, and can survive for decades in ambient conditions. Extrapolation from primate studies have shown that between 1 and 3 of these spores may be sufficient for an infection (Inglesby 2002). Unfortunately, current immunoassay–biosensor limitations lack the sensitivity and specificity for proper *B. anthracis* spore detection (Service 2005). Hence, device improvement for the detection of such pathogens is of paramount importance.

Although there are a number of different designs to improve immunoassay–biosensor capabilities, one approach that has not received much attention to date is to mimic the nanostructure surface roughness of cells from our own immune system. Clearly, our own immune system has been optimized for antigen–antibody capture. For example, the avidity of the non-covalent interactions on a B-lymphocyte's membrane suggests that

Correspondence: Thomas J Webster
Division of Engineering,
Brown University, Box D, Providence,
RI 02912, USA
Phone +1 401 863 2361
Fax +1 401 863 1141
Email thomas_webster@brown.edu

many properties (such as flexibility, charge, and roughness) may promote antigen capture. Several studies have observed and reported the nanometer membrane topography of a lymphoid cell using atomic force microscopy (Damjanovich et al 1995; Cricenti et al 1999; Sakaue and Taniguchi 2001) or scanning electron microscopy (Setum et al 1993).

It should not be surprising that our own immune cells have highly nanostructured membranes due to the presence of membrane-linked proteins, phospholipid bilayers, and other bioactive molecules. Thus, it should also not be surprising that computational modeling has proposed that promoting surface roughness may be one way to enhance antigen capture on immunoassay–biosensor surfaces through enlarged antigen contact surface area (Zheng and Rundell 2003). In addition to increased surface area, nanoscale roughness on materials allows for unique energetics through greater portions of surface defects and altered electron delocalizations.

Because of this, nanometer surface roughness has been shown to influence the behavior of many cell types. For example, studies have demonstrated increased adhesion and growth of endothelial cells (Miller et al 2004), smooth muscle cells (Miller et al 2004), neurons (Ejiofor et al 2004), osteoblasts (Price et al 2003), and leukocytes (Eriksson et al 2001) on nanometer compared with micron rough surfaces. Surface topography causes modulation of chemokines and cytokines in macrophages (Refai et al 2004), activation of platelets and monocytes (Hsu et al 2004), and changes in the locomotion of different T cell types (Mello et al 2003). Although showing promise for implant/tissue engineering applications, the use of nanometer surface roughness on immunoassay–biosensor membranes for enhancing antigen-antibody capture remains largely uninvestigated.

For all of the above reasons, the objective of the present study was to investigate antigen capture on model immunoassay–biosensor surfaces of varying degrees of nanometer roughness. It is proposed that this biologically inspired nanometer surface roughness is one factor that naturally promotes antigen–antibody interactions which has yet to be explored in current immunoassay–biosensor designs.

Materials and methods
Immunosurface preparation
To determine the size of particles that should be used to model the surface roughness of B-lymphocytes, imaging software (ImageJ) was employed to evaluate the change in surface area (that is, the ratio of the outlined surface area of the cell membrane to that of a circle) of a B-lymphocyte

from an image provided in the literature (Roitt et al 1993). The percentage change in surface area was calculated to be 1.851431±0.034405 (average±SEM) This value was close to what could be obtained by using 860-nm diameter particles placed on flat immunosurfaces; particles of two additional sizes (specifically, 40 and 460 nm) were added in this study for comparison purposes.

The model immunosurfaces were constructed in three layers through physisorption. IgG antibodies comprised the first layer, the second layer consisted of either Protein A (PA) or PA conjugated particles, and the third layer contained the second antibody layer (Figure 1). The surface roughness was controlled by the size and surface density of the immobilized PA conjugated particles. All layers were constructed at room temperature (27°C). Throughout this immunosurface construction procedure, the samples were not allowed to dry to avoid non-uniformity (Hayes 1998).
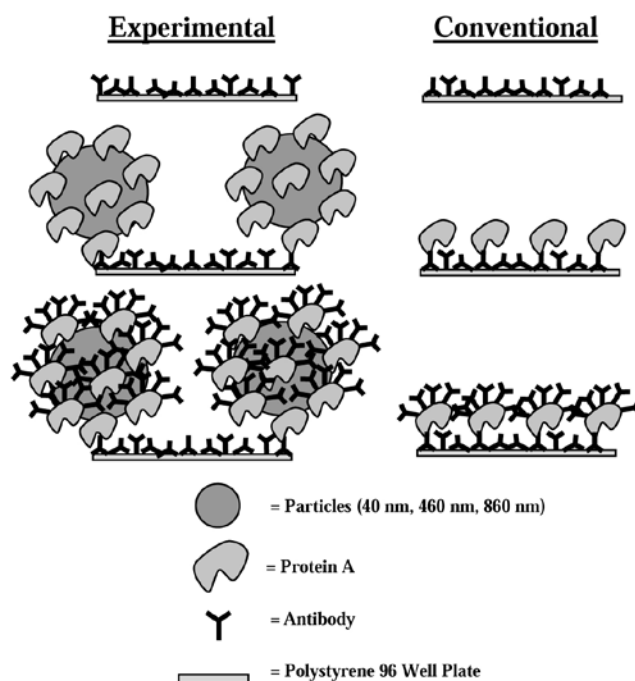

Figure 1 Model immunoassay surface construction. Experimental (left) and conventional (right) immunoassay surface construction scheme.

Construction of layer 1
In the present study, mouse IgG2aαDNP (anti-2,4-dinitrophenol, kappa specific; Accurate Chemical) antibodies were used for the active surfaces and non-specific mouse IgG2a (kappa specific; Sigma) antibodies were used for the inactive surfaces. These antibodies were diluted in 1X phosphate-buffered saline (PBS) without ions (4.0 g NaCl, 0.1 g KCl, 0.75 g Na_2HPO_4, and 0.1 g KH_2PO_4 added to 500

mL Milli-Q water, pH adjusted to 7.4) to a final concentration of either 11.1, 6.7, or 3.3 μg/mL. 50 μL of this antibody solution was aliquoted to each sample well of a 96-well plate (polystyrene, flat bottom without lid, high binding, non-sterile, EIA/RIA; Corning). The antibodies were adsorbed to the polystyrene surface for 1 hour. Samples were gently rinsed 5 times with 200 μL of PBS in each well. The adsorption of the initial antibody layer results in a random orientation (Lu et al 1996), leaving some correctly oriented accessible Fc regions for the secondary attachment of PA.

Construction of layer 2

The second layer consisted of either PA (Sigma) or PA conjugated particles. The PA for the conventional surface was diluted in PBS to a final concentration of 4 μg/mL. 50 μL of the PA solution was adsorbed for 20 min and was gently washed 5 times with 200 μL of PBS in each well. The PA conjugated particles included 40-nm gold particles (OD=10.1; Ted Pella, Inc), 460-nm yellow fluorescent polystyrene particles (0.1 % w/v; Spherotech, Inc), and 860-nm polystyrene particles (1.0 % w/v; Spherotech, Inc). PA conjugated particle concentrations were used at stock solution concentrations (8.7×10^{11} particles/mL, 18.0×10^{9} particles/mL, and 14.0×10^{9} particles/mL for the 40, 460, and 860 nm particles, respectively). To ensure that the only protein in the solution was PA conjugated to the particles, each solution was microcentrifuged (Model V, VWR) at 5585 xg at 4°C for 12 min, whereby the supernatant was removed and replaced with an equal volume of PBS. After replacement of the supernatant, the preparation was vortexed at 3200 rpm (speed setting 10) (Mini Vortexer, VWR) and was sonicated for 2 min (Aquasonic 75T, 90 W, VWR) to resuspend the particles in solution. This procedure was repeated twice. 50 μL of the final particle solution was adsorbed onto the first layer of antibodies overnight. Alternatively, 50 μL of the final particle solution was further diluted from this stock solution in PBS to the desired dilution factor (1:0, 1:10, 1:100, 1:1000, and 1:10,000) which was then adsorbed overnight. The 96-well plate was covered with a lid as much as possible to avoid evaporation and contamination. After the particles adsorbed overnight, the samples were gently washed 5 times with 200 μL PBS in each well.

Construction of layer 3

The second antibody layer, either specific or non-specific, was adsorbed to form the third and final layer of the model immunoassay surface. The procedure for the third layer was identical to that for the first layer. The PA on the second layer

served to correctly orient the antibodies through binding of PA to the Fc region of the antibody, allowing the Fab regions to be accessible to the antigen.

Immunosurface characterization
AFM measurements of surface roughness
Atomic force microscopy (AFM) was used to determine the topology and roughness of the various surfaces created in the present study. Specifically, samples were prepared for AFM by constructing only the first two layers of the immunoassay membrane (as described above). Samples were mounted using double-stick tape (3M) onto 12-mm mica specimen discs (Ted Pella, Inc.) and were imaged using a Veeco Nanoscope IIIa MultiMode scanning probe microscopy (SPM) in Tapping™ mode. Standard AFM tips and measuring conditions (thickness: 4 μm, width: 30 μm, length: 125 μm, force constant: 42 N/m, resonance frequency: 320 kHz) were used in non-contact/Tapping™ mode with a reflexive coating (Pacific Nanotechnology). Three AFM 5x5 μm scans at 512x512 lines per image were taken for each sample, for 3 different samples of each surface type, at a rate of 1 Hz and a velocity of 10 μm/s. The average room temperature during imaging was 24°C with an average humidity of 30%–40%. Three types of roughness measurements were calculated using Nanoscope IIIa 4.43r8 software in this study: root-mean-square roughness (RMS), average surface roughness (Ra), and the change in surface area (ΔSA) or Wenzel ratio. Three-dimensional topographic images were constructed using WSxM 4.0 Develop 4.4 software (Nanotec Electronica S.L.).

Hydrophilicity measurements
To determine hydrophilicity of the model immunoassay membranes, static contact angles were measured (Cam-Plus Contact Angle Reader, Tantec) in triplicate. In this manner, contact angles on each of the surfaces of interest to the present study (including the conventional surfaces) were measured immediately after adding 1 μL of Milli-q water using the Sessile Drop, Half-Angle™ Tangent line method (Tantec).

Protein A quantification
An estimate of the PA surface density was obtained for the different immunosurface constructs by multiplying the amount of PA determined per particle times the surface density of the particles as determined from the above mentioned 5x5 μm AFM scans. A well-established BCA™ (Pierce) commercially available technique was used to determine the amount of PA per particle from stock solutions of a known concentration of particles.

Functionality of immunosurfaces: antigen binding

Undoubtedly, the most important characteristic of an immunoassay–sensor is its ability to bind antigen. To test this, the functionality of the immunosurface was assessed by considering both specific and non-specific antigen capture. Antigens were modeled as microspheres (MSs) in the present study. Specific antigen interactions were quantified by the number of bound active MSs (DNP-BSA) to the immunosurfaces constructed with specific antibodies (IgG). Three types of non-specific interactions were investigated: (1) non-specific antibody (IgG (NS)) surfaces exposed to active and (2) control MSs, and (3) specific antibody (IgG) surfaces exposed to control MSs. Only active MS non-specific binding was reported due to space limitations as the other two types of non-specific binding were always less than this value. The various surface types were constructed as described above and the antigens were constructed and exposed to the immunosurfaces as described in the sections that follow.

Antigen preparation

The antigen used for testing the functionality of the immunosurfaces for both specific and non-specific binding was an antigenic complex of DNP conjugated to bovine serum albumin (BSA) (Molecular Probes with a valency of 22.8) adsorbed onto carboxylate-modified, 1 μm polystyrene Nile red fluorescent MSs (Excitation: 535 nm, Emission: 575 nm; FluoSpheres, Molecular Probes); this created active MSs for testing specific binding to the various immunosurfaces. For this purpose, lyophilized DNP-BSA powder was reconstituted in PBS to form a DNP-BSA solution concentration of 1.25 mg/mL, where the fluorescent MSs (2.0% solids stock) were added at a ratio of 1:20, vortexed at 3200 rpm, and allowed to sit in the dark at 4°C for 2 days to allow for the adsorption of the antigen (DNP-BSA) onto the fluorescent MSs. The MS/DNP-BSA solution was then microcentrifuged at 5585 xg at 4°C for 20 min, whereby the derivatized MS pellet was washed and resuspended by vortexing with PBS. The resuspended MS/DNP-BSA solution was allowed to sit and cure for at least 3 days at 4° C in the dark to stabilize the MS/DNP-BSA interaction. Control microspheres for testing non-specific binding were constructed from BSA adsorbed to the MSs, prepared using the procedure mentioned above with 1.25 mg/mL BSA replacing the DNP-BSA solution.

Quantifying antigen capture on immunosurfaces

Following the construction of the various immunosurfaces, 50 μL (2.4×10^6 MS) of active (DNP-BSA) or control (BSA) MSs were exposed to the various immunosurfaces in the 96

well plate for 10 min. 50 μL of each solution of active and control MSs were produced from an overall 1.15 mL solution that consisted of 30 μL of the respective stock solution in 1 mL of PBS and 120 μL of BlockAid™ (Molecular Probes). BlockAid™ is a proprietary protein solution which limits non-specific binding when using Molecular Probes MSs (Molecular Probes Product Information, 2001). After the MSs were allowed to interact with the immunosurfaces for 10 min, samples were gently rinsed 5 times with 200 μL of PBS in each well. One image per well (within the center) was collected using an inverted fluorescent microscope (Leica DM IRB) equipped with Texas red isothiocyanate (TRITC)-compatible filters (BP 515–560, LP 590, Leica) and a capacitive coupled display (CCD) camera at 10x magnification. Bound MSs were counted using ImagePro Plus software.

Statistical analyses

Analysis of variance (ANOVA) with a variance stabilization procedure was performed to determine differences between the surfaces of interest to the present study. Experimental data (reported as average ± SEM)) were analyzed using Tukey's procedure (the T method). A two-sample t-test was used in a few cases in which unequal sample sizes existed.

Results and discussion
Immunosurface characterization: roughness

As expected, large differences in surface roughness were observed through the use of the various particle sizes in the present study (Figure 2 and Table 1). Most importantly, results demonstrated increased surface roughness through the addition of particles to the polystyrene wells. Specifically, the highest degree of roughness was observed with the use of 860-nm followed by 460-nm followed by 40-nm diameter particles; all had greater surface roughness than polystyrene alone. As a reminder, the type of surface roughness that best modeled that of a B-lymphocyte from an image provided in the literature (Roitt et al 1993) was through the use of 860-nm diameter particles.
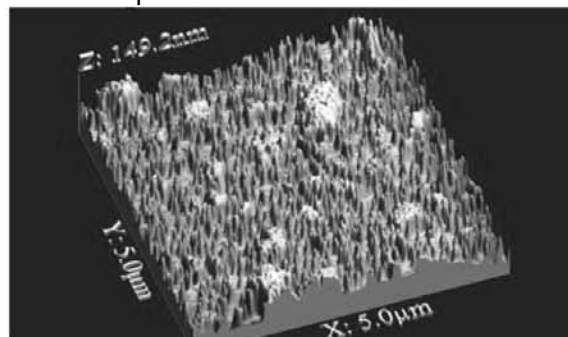
Immunosurface characterization: antigen binding

Results of this study provided evidence that specific antigen capture increased as the surface roughness increased, while non-specific antigen capture was independent of surface roughness (Figure 3). The change in surface roughness data
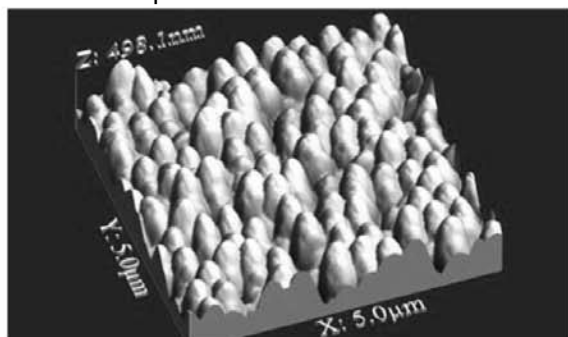
A. Polystyrene alone
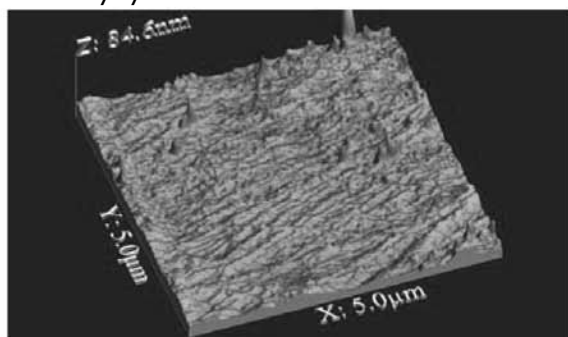
B. 40 nm particles

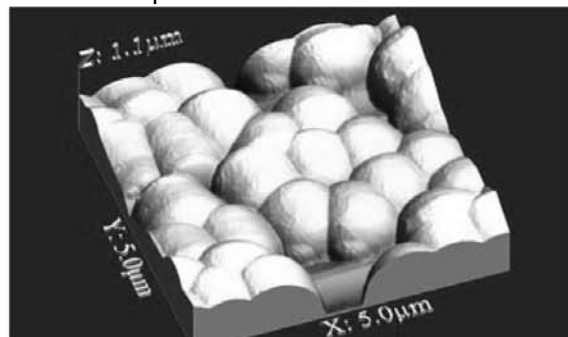C. 460 nm particles

D. 860 nm particles

Figure 2 3D AFM images of immunoassay surfaces. AFM 3D surface images with physisorbed antibody concentrations of 11.1 µg/mL obtained using tapping mode in air on a (A) conventional 96-well polystyrene plate alone, (B) 40-nm gold nanoparticles conjugated with Protein A attached to a 96-well plate, (C) 460-nm polystyrene particles conjugated with Protein A attached to a 96-well plate, and (D) 860-nm polystyrene particles conjugated with Protein A attached to a 96-well plate.

Table 1 Surface roughness summary

Particle Size	Surface roughness measurement	Surface roughness variations (data = mean ±SEM)					
		Control (conventional)	Particle serial dilutions				
			1:0	1:10	1:100	1:1000	1:10,000
40 nm	RMS (nm)	4.073 ±0.259	23.357 ±3.102	11.933 ±1.372	4.478 ±0.211	2.665 ±0.129	3.167 ±0.356
	Ra (nm)	2.949 ±0.199	18.714 ±2.623	7.319 ±1.045	2.775 ±0.433	1.898 ±0.082	2.173 ±0.116
	$\triangle$ SA	1.011 ±0.004	1.239 ±0.012	1.075 ±0.007	1.023 ±0.003	1.016 ±0.002	1.013 ±0.002
460 nm	RMS (nm)	4.073 ±0.259	92.129 ±3.157	98.384 ±5.251	29.958 ±5.539	4.238 ±1.110	3.425 ±0.667
	Ra (nm)	2.949 ±0.199	73.524 ±2.701	69.264 ±6.456	10.666 ±1.824	2.359 ±0.227	2.127 ±0.124
	$\triangle$ SA	1.011 ±0.004	1.302 ±0.016	1.147 ±0.014	1.023 ±0.007	1.000 ±0.001	0.999 ±0.001
860 nm	RMS (nm)	4.073 ±0.259	203.39 ±7.564	237.062 ±4.897	103.267 ±28.351	29.422 ±17.646	2.549 ±0.213
	Ra (nm)	2.949 ±0.199	159.32 ±8.173	195.777 ±4.667	64.364 ±20.848	20.922 ±14.703	1.968 ±0.201
	$\triangle$ SA	1.011 ±0.004	1.401 ±0.013	1.589 ±0.025	1.127 ±0.037	1.043 ±0.018	1.002 ±0.002

Abbreviations: RMS, root-mean-square roughness; Ra, average surface roughness; $\triangle$SA, change in surface roughness or Wentzel ratio; Control (conventional), no particles used.
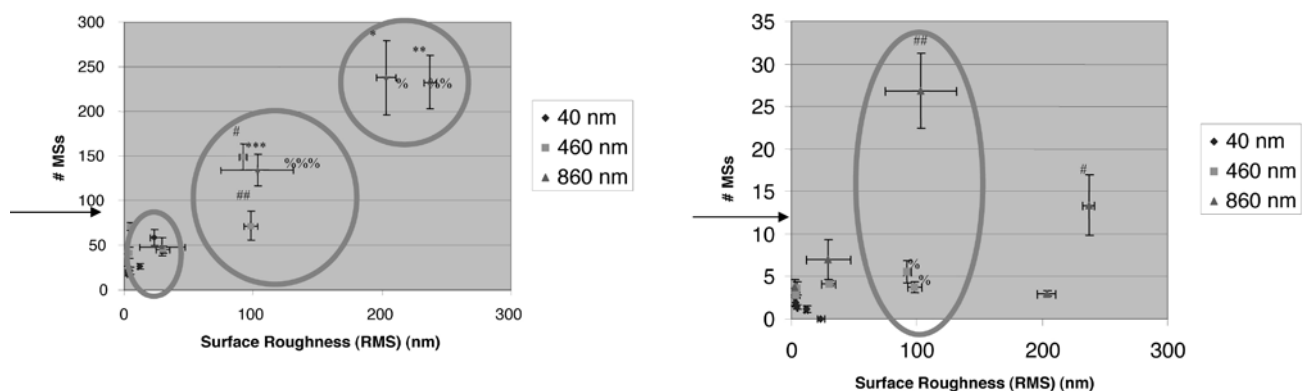
Figure 3 (Left) Increased specific antigen capture with increased surface roughness; (Right) non-specific binding independent of surface roughness. (Top) The circles highlight the change in specific antigen capture at the 100- and 200-nm (RMS values) surface roughness regimes emphasizing the statistical increase in specific antigen capture with greater surface roughness. The conventional surfaces (polystyrene plate alone) allowed for the attachment of 76.13±21.15 microspheres (MSs; indicated by the arrow). Data = mean ± SEM.
Statistics: 860-nm 1:0 active MS surface is statistically significantly different from all 860-nm surfaces except 1:10 with p<0.01 (*). 860-nm 1:10 active MS surface compared with all 860-nm surfaces except 1:0 with p<0.01 (**). 860-nm 1:100 and conventional active MS surfaces compared with 860-nm 1:1000 and 1:10000 surfaces with p<0.01 (***). 460-nm 1:0 active MS surface is statistically significantly different from all 460 nm surfaces with P<0.01 (#). 460-nm 1:10 active MS surface compared to 460-nm 1:100 and 1:10000 surfaces with p<0.01 (##). RMS 460-nm 1:0 (%) and 1:10 (%%) are statistically significantly different from all other 460-nm surfaces except each other with p<0.01. RMS 460-nm 1:100 (%%%) compared with all other 460-nm surfaces with p<0.01.
(Right) The circle highlights the change in nonspecific antigen capture at the 100 nm surface roughness regime. The conventional surfaces allowed for the attachment of 11.00±8.11 MSs (indicated by the arrow). Data = mean ± SEM.
Statistics: 860-nm 1:10 control MS surface compared with 1:100 surface with p<0.01 (#). 860-nm 1:100 control MS surface compared with 1:1000 and 1:10000 surfaces with p<0.01 (##). RMS 460-nm 1:0 (%) and 1:10 (%) are statistically significantly different from all other 460-nm surfaces except each other with p<0.01.
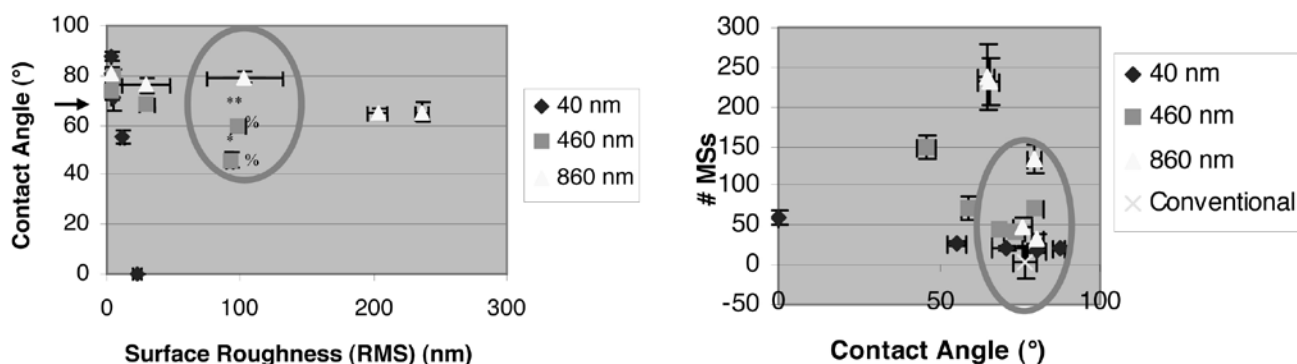

Figure 4 (Left) Changing contact angles within similar immunoassays surface roughness values; (Right) antigen capture independent of surface energetics. (Left) Circle highlights different surface energetics at the 100-nm surface roughness regime due to similar roughness values (RMS) but altered contact angles. The conventional surface contact angle, indicated by an arrow, was 76.67±3.52°. Results showed that the 40-nm particle surface decreased contact angles at the highest rate (−3.9203°/nm), the 460-nm particle surface decreased at an intermediate rate (−0.2542°/nm), and the 860-nm particle surface decreased at the slowest rate (−0.0661°/nm). Data = mean ± SEM.
Statistics: 460-nm 1:0 compared with all other 460-nm surfaces with p<0.01 (*). 460-nm 1:10 compared to all other 460-nm surfaces with p<0.01, except 1:100 with p<0.1 (**). RMS 460 nm 1:0 (%) and 1:10 (%) are statistically significantly different from all other 460-nm surfaces except each other with p<0.01.
(Right) Circle highlights change in specific antigen capture without a change in surface energetics as measured by contact angles. Data = mean ± SEM. Conventional = polystyrene alone (without particles).

within each surface type reflects the serial dilutions of the particles (1:0, 1:10, 1:100, 1:1000, and 1:10000). These data showed that even though surface roughness may be a factor, there are likely other factors involved in mediating antigen capture, such as surface chemistry changes or alterations in PA surface density. This is likely since at the 100-nm surface roughness regime there is a difference in specific and non-specific antigen capture between surface types. This can be further confirmed in Figure 4 where at the 100-nm surface roughness regime the surface types have different energetics, as determined through contact angle measurements. This may

be due to a change in surface chemistry from the different types of polystyrene particles used and/or the different amounts of PA conjugated on those particles. Moreover, in Figure 4 it can be seen that within each immobilized particle type, the surface energetics change as the surface roughness changes.

It is important to note that Figure 4 complements Figure 3 since collectively they show that when either surface roughness or surface energetics (that is, contact angles) were held constant, there was still a change in specific and nonspecific antigen capture. That is, specific and non-specific antigen capture is most likely due to a combination of a

change in surface chemistry and surface roughness, with surface roughness playing a larger role in specific antigen capture than non-specific antigen capture.

To investigate further what properties may have changed when using the more rough surfaces (that is, those with 860-nm particles), surface chemistry differences possibly due to various amounts of PA were evaluated. Results provided evidence that the density of PA was not correlated with surface roughness and that specific and non-specific antigen capture did not depend solely on the density of PA on the surface (Figure 5). Specifically, the 460- and 860-nm particle surfaces had similar amounts of PA yet the 860-nm particle surface enhanced antigen capture. As seen in Figures 3 and 4, this again suggests that the surface roughness created in this study through the use of various nanometer particle sizes did not cause different surface energetics that manipulated protein density.

When analyzing different physisorbed antibody concentrations, the disproportionate increases in specific antigen capture on the 860-nm particle surface may be explained due to a greater amount of antibody immobilized and/or a greater functionality of those immobilized antibodies (Figure 6). Comparison of Figures 3, 4, and 5 highlights the possibility that it may not just be the amount of IgG adsorbed
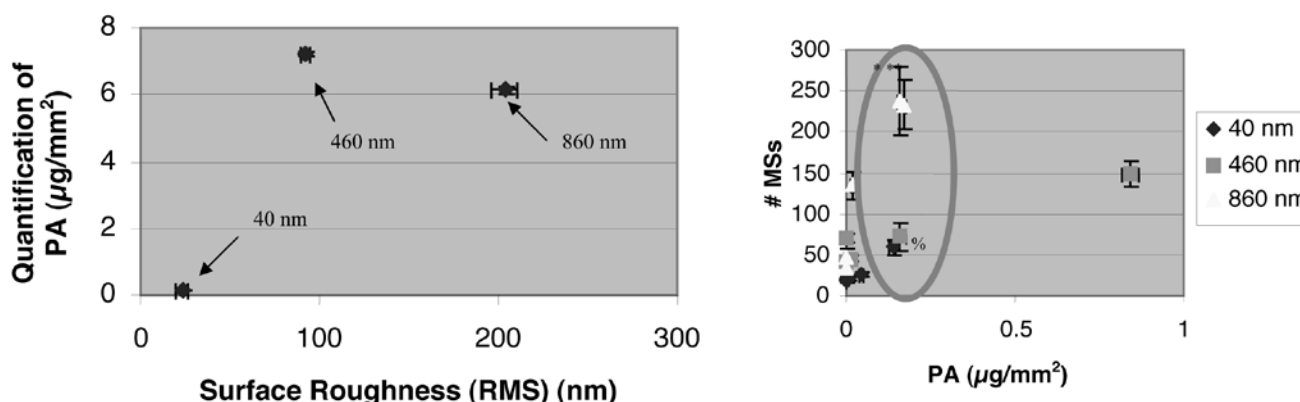

Figure 5 (Left) PA surface density did not depend on surface roughness; (Right) specific antigen capture did not depend on pa surface density. (Left) The 40-nm particle surface is the left data point, the 460-nm particle surface is the middle data point, and the 860-nm particle surface is the right data point. The conventional (or polystyrene alone) immunosurface PA density was 0.004146 ± 0.0022 µg/mm^2 (mean ± SEM). Since similar PA densities were measured for the 460- and 860-nm particles, results were provided that PA surface density did not depend on surface roughness. Data = mean ± SEM.
Statistics: All surfaces statistically significant different to each other with $p<0.01$ with respect to surface roughness (RMS) and PA density.
(Right) Circle highlights the change in specific antigen capture without a change in PA density. Data = mean ± SEM.
Statistics: 860-nm 1:0 active MS surface is statistically significantly different from all 860-nm surfaces except 1:10 with $p<0.01$ (*). 860-nm 1:10 active MS surface compared to all 860-nm surfaces except 1:0 with $p<0.01$ (**). There is statistically no difference between the PA densities of the four points within the oval (%).
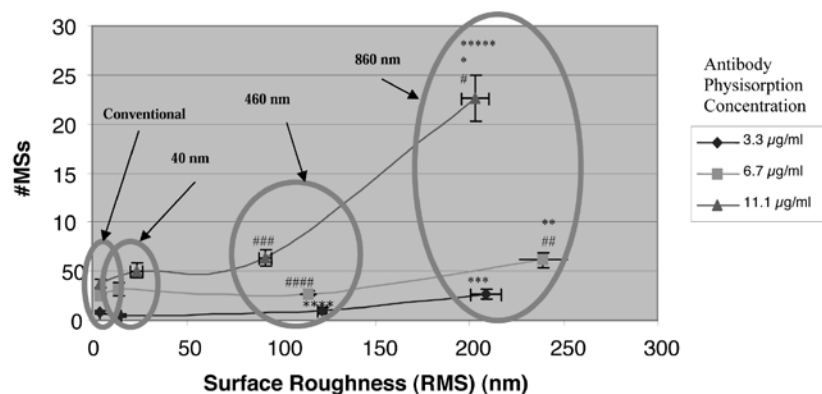

Figure 6 Increased specific antigen capture with greater surface roughness and greater physisorption of antibodies. Surface types are at stock (1:0) levels. Each circle represents similar surface types with different physisorbed antibody concentrations. A disproportionate increase in specific antigen capture was seen with respect to greater surface roughness and physisorbed antibody concentrations. Specific antigen capture at antibody physisorbed concentrations of 11.1 µg/mL increased by approximately 540% when the surface roughness (RMS) increased by approximately 1900% (that is, going from conventional or polystyrene alone surfaces to those with 860 nm particles). Data = mean +/- SEM.
Statistics: Statistical grouping by 11.1 µg/mL, 6.7 µg/mL, 3.3 µg/mL physisorbed Abs, and all data. 11.1 µg/mL active MSs 860-nm surface is statistically significantly different frp, all surfaces with $p<0.01$ (*). 6.7 µg/mL active MSs 860-nm surface compared with all surfaces with $p<0.01$ (**). 3.3 µg/mL Active MSs 860-nm surface compared with all surfaces with $p<0.01$ (***). 3.3 µg/ml active MSs 460-nm surface compared with 40-nm surface with $p<0.1$ (****). Within all data 11 µg/ml 860-nm compared with all surfaces with $p<0.01$ expect for with the 6.7 µg/mL 860-nm with $P<0.05$ (*****). N=20 for 11.1 µg/mL, N=5 for 6.7 µg/mL and 3.3 µg/mL. Statistical grouping by particle type. 11.1 860-nm compared with 6.7 and 3.3 860-nm with $p<0.01$ (#), 6.7 860-nm compared to 3.3 860-nm with $p<0.05$ (##). 11.1 460-nm compared with 6.7 and 3.3 460-nm with $p<0.01$ (###), 6.7 460-nm compared with 3.3 460-nm with $p<0.01$ (####). N=20 for 11.1 µg/ml, N=5 for 6.7 µg/ml and 3.3 µg/ml.

but the functionality of those adsorbed antibodies, since the most specific binding was not found on the surface with the most PA.

Reasons for altered antigen binding

When surface roughness and surface chemistry are both changed, as was done here, it is difficult to determine to what extent each variable is contributing to specific and nonspecific antigen capture. However, the results of the present study demonstrated that surface roughness is an important parameter for increasing antigen capture. Moreover, the largest specific antigen capture was seen when 860-nm particles were used on the immunoassay surfaces, which corresponded to the aforementioned estimate of the surface roughness of a B-lymphocyte membrane.

In this manner, one explanation of why antibody functionality may be enhanced when immobilized on increasingly roughened immunosurfaces may lie with the probabilistic geometrical nature of a roughened surface. That is, various non-covalent forces govern every antigen–antibody binding event. These different forces vary in strength depending on the distance between an antigen and an antibody. It can then be rationalized that the surface area of an immunoassay–sensor is mirrored in solution due to these varying forces. Thus, a more rough immunoassay surface may result in a more rough mirrored antigen contact area created by the non-covalent forces within the solution. Probabilistically, antigens in solution will be more likely to interact with these non-covalent forces to result in specific antigen capture. In other words, the functionality of the individual antibodies may not be intrinsically enhanced, but the collective whole of the antibodies on the immunosurface may be enhanced.

Conclusions

In conclusion, this study provided evidence that nanometer surface roughness may be a critical design parameter for future immunoassays–sensors since the sensitivity of an antibody–antigen capture may be enhanced without an increase in non-specific binding. An increase in nanometer surface roughness was observed in this study through the use of larger immobilized particles. It then followed that a decrease in surface roughness was created through serial dilutions of those immobilized particles. Greater specific antigen capture correlated with increased surface roughness and physisorbed antibody concentrations, while nonspecific antigen capture was independent of surface roughness. Surface energetic experiments involving contact angles

suggested that there might be a change in surface chemistry between the different immunoassay surface types. However, even amidst a possible surface chemistry change, results of this study implied that nanometer surface roughness was the dominating factor that contributed to greater specific antigen capture. Such knowledge of the use of nanostructured surface roughness should be used to design better immunoassays/biosensors.

References

Cricenti A, Generosi R, Girasole M, et al. 1999. Atomic force microscopy observation of human lymphoid cells chronically infected with the human immunodeficiency virus. *J Vac Sci Technol A*, 17:1141-4.

Damjanovich S, Vereb G, Schaper A, et al. 1995. Structural hierarchy in the clustering of hla class-i molecules in the plasma-membrane of human lymphoblastoid-cells. *Proc Natl Acad Sci U S A*, 92:1122-6.

Ejiofor JU, Waid MC, McKenzie JL, et al. 2004. Nano-biotechnology: carbon nanofibres as improved neural and orthopaedic implants. *Nanotechnology*, 15:48-54.

Eriksson C, Lausmaa J, Nygren H, 2001. Interactions between human whole blood and modified TiO2-surfaces: Influence of surface topography and oxide thickness on leukocyte adhesion and activation. *Biomaterials*, 22:1987-96.

Hayes K, Badly, Cullen, 1998. AFM Study of Antibody Adsorption to Polystyrene Microtitre Plates. *Nanobiology*, 4:141-51.

Hsu SH, Tang CM, Lin CC, 2004. Biocompatibility of poly(epsilon-caprolactone)/poly(ethylene glycol) diblock copolymers with nanophase separation. *Biomaterials*, 25:5593-601.

Inglesby TV. 2002. Anthrax as a biological weapon, 2002: Updated recommendations for management. *JAMA*, 288:1849.

Lu B, Smyth MR, Okennedy R, 1996. Oriented immobilization of antibodies and its applications in immunoassays and immunosensors. *Analyst*, 121:R29-R32.

Miller DC, Thapa A, Haberstroh KM, et al. 2004. Endothelial and vascular smooth muscle cell function on poly(lactic-co-glycolic acid) with nano-structured surface features. *Biomaterials*, 25:53-61.

Mello AP, Volkov Y, Kelleher D, et al. 2003. Comparative locomotory behavior of T lymphocytes versus T lymphoma cells on flat and grooved surfaces. *Ann Biomed Eng*, 31:1106-13.

Price RL, Gutwein LG, Kaledin L, et al. 2003. Osteoblast function on nanophase alumina materials: Influence of chemistry, phase, and topography. *J Biomed Mater Res A*, 67A:1284-93.

Refai AK, Textor M, Brunette DM, et al. 2004. Effect of titanium surface topography on macrophage activation and secretion of proinflammatory cytokines and chemokines. *J Biomed Mater Res A*, 70A:194-205.

Roitt IM, Brostoff J, Male DK. 1993. Immunology. 3rd ed. St. Louis: Mosby.

Sakaue M, Taniguchi K, 2001. Imaging of the lectin-labeled cell surface of human lymphocytes by the use of atomic force microscope. *J Vet Med Sci*, 63:223-5.

Service RF. 2005. Fast, sensitive scan targets anthrax. *Science*, 308(5718):45.

Setum CM, Serie JR, Hegre OD, 1993. Dendritic cell lymphocyte clustering - morphologic analysis by transmission electron-microscopy and distribution of gold-labeled mhc class-ii antigens by high-resolution scanning electron-microscopy. *Anat Rec*, 235:285-95.

Zheng YN, Rundell AE, 2003. Biosensor immunosurface engineering inspired by B-cell membrane-bound antibodies: Modeling and analysis of multivalent antigen capture by immobilized antibodies. *IEEE Trans Nanobioscience*, 2:14-25.